NeuroImage: Clinical 36 (2022) 103272

Contents lists available at ScienceDirect

NeuroImage: Clinical

journal homepage: www.elsevier.com/locate/ynicl

Highest resolution microCT scan of the human brainstem reveals putative anatomical basis for infrequency of medial medullary syndrome

Kaylea M. Feldman [a,*], Yasmin A. O'Keefe [b], Paul M. Gignac [a,c], Haley D. O'Brien [a,c,*]

[a] Oklahoma State University Center for Health Sciences, Department of Anatomy and Cell Biology, 1111 W 17th Street, Tulsa, OK 74107, USA
[b] Ascension St. John Medical Center, Department of Neurology/Neurocritical Care, 2100 S Wheeling Ave, Tulsa, OK 74104, USA
[c] University of Arizona, Department of Cellular and Molecular Medicine, 1501 N. Campbell Avenue, PO Box 245044, Tucson, AZ 85724, USA

ARTICLE INFO

Keywords:
Medial medullary syndrome
Déjerine Syndrome
diceCT
Anterior spinal artery
High-resolution imaging
MicroCT scanning
Ischemic stroke

ABSTRACT

Ischemic strokes affecting the medial medulla are exceedingly rare. The anatomical basis for the relative infrequency of this stroke syndrome has been largely uninvestigated due to historically coarse MRI and CT scan resolution. We capture and digitally dissect the highest-ever-resolution diffusible iodine-based contrast-enhanced CT (diceCT) scanned images of a cadaveric brainstem to map arterial territories implicated in medial medullary infarctions. 3D reconstructions show that within the anterior spinal artery territory previously implicated in medial medullary syndrome (MMS), there are numerous, small sulcal artery branches perforating the medulla within the anterior median fissure. These branches proceed in parallel through the anteroposterior depth of the medulla as expected; however, we also identify a network of intraparenchymal, rostrocaudal anastomoses between these sulcal perforating branches. This network of intraparenchymal sulcal artery anastomoses has never been described and may provide a significant collateral supply of oxygenated blood flow throughout the medial medulla. By ramifying deeper tissues, these anastomoses can help explain the infrequency of MMS.

1. Introduction

Posterior circulation ischemic strokes account for approximately 20–25 % of acute ischemic strokes (Merwick and Werring, 2014). Derived primarily from the vertebral and basilar arteries, posterior circulation strokes affect the brainstem, with syndromes relating to arterial territories in the medial or lateral divisions of the midbrain, pons, or medulla. Although ischemic strokes are known to affect each of these six brainstem regions, medial medullary strokes are the most rare, making up approximately 1 % of reported cases (Basetti et al., 1997; Fukota et al., 2012; Toyoda et al., 1996). Infarctions of the medial medulla, otherwise known as medial medullary syndrome (MMS), or Déjerine Syndrome, are primarily attributed to atherothrombotic occlusion of the anterior spinal, vertebral, or caudal basilar arteries and their branches (Fukota et al., 2012; Kim et al., 1995). Infarctions in this territory characteristically damage structures of the anteromedial medulla including the lateral corticospinal tracts, medial lemniscus, and hypoglossal nerve and nucleus. Injury to these structures explains the clinical syndrome of MMS, composed of hemiparesis and hemisensory deficits, both sparing the face, contralateral to the lesion, and tongue paralysis ipsilateral to the lesion. It should be noted that these classical neurological symptoms are unlikely to all be present at onset, and have been shown to be variably accompanied by additional semiology such as nystagmus (due to damage to the medial longitudinal fasciculus and nucleus prepositus hypoglossi), and/or headache (Fukota et al., 2012; Toyoda et al., 1996; Kim et al., 1995). Due to the combination of bilaterally paired (e.g. vertebral) and midline, unpaired (e.g. anterior spinal and basilar) arteries implicated in MMS, the clinical syndrome can present unilaterally or bilaterally, respectively. A unilateral syndrome with involvement of the vertebral or basilar arteries and their branches represents the more common condition. The less common bilateral syndrome represents involvement of the anterior spinal artery and its perforators (Toyoda et al., 1996; Kim et al., 1995). Further, of the three rostrocaudal divisions of the medulla delineated by Kim (2003), Currier et al. (1961), and Vulleumier et al. (1995), MMS appears to occur least frequently in the lower medulla (Fukota et al., 2012).

The relative infrequency of MMS is of particular interest when compared to the incidence of ischemic stroke in other small vessel and perforating arterial territories. Anatomically speaking, the small luminal diameter and prevalence of acute and right-angle branching observed in

Abbreviations: ASA, anterior spinal artery; HN, hypoglossal nucleus; ML, medial lemniscus; PMD, pyramid; VA, vertebral artery.

* Corresponding authors at: 1501 N. Campbell Avenue, PO Box 245044, Tucson, AZ 85724-5044, USA (H. O'Brien).
E-mail addresses: kaylea.bixler@okstate.edu (K.M. Feldman), haleyobrien@arizona.edu (H.D. O'Brien).

https://doi.org/10.1016/j.nicl.2022.103272
Received 13 July 2022; Received in revised form 1 November 2022; Accepted 17 November 2022
Available online 18 November 2022

small vessel and perforating arterial territories renders them more susceptible to increased wall stress and subsequent occlusion. This intrinsic susceptibility is corroborated by the frequency of infarction in similar small, perforator-type vessels: lacunar infarctions, or infarctions of the penetrating branches of the larger cerebral arteries, have in fact been shown to comprise 13–48 % of all strokes in a given population (Kim et al., 1994; Paciaroni et al., 2003; Ng et al., 2007). Similarly, ischemic strokes of paramedian pontine branches of the basilar artery comprise approximately 8 % of all strokes in a population, and a disproportionately high 28 % of all vertebrobasilar infarcts (Kataoka et al., 1997). The disparity in frequency between the regions described above and that of the medial medulla largely remains unexplained. Investigation of an anatomical basis for this disparity has historically been limited by an unfavorable ratio of fine blood vessel size to coarse MRI and CT scan resolution. Here, we aim to elucidate a putative anatomical basis for the low incidence of MMS using the highest-ever-resolution CT imaging of a cadaveric brainstem to visualize arteries of the medial medulla.

2. Methods

2.1. Staining

Four non-pathologic, cadaveric brains of Oklahoma State University Center for Health Sciences body donors ($N_{female} = 2$, $N_{male} = 2$; *ages*: average = 72.25; range: 62–83) were fixed in formalin and soft-tissue contrast stained using a 3 % concentration of Lugol's iodine (I_2KI) for 12.5 weeks (refreshed every 2 weeks). The I_2KI solution was agitated when samples were first added and during each refreshment to ensure that the solution entered the sulci of the brain. Further, brains were rotated 180° every week to ensure that regions in contact with the bottom of the container were sufficiently stained. Light was prevented from reaching the staining container to ensure that solution strength did not break down due to light exposure (Gignac et al., 2016). This process of soft-tissue contrast enhancement is the first step of the process commonly known as diffusible iodine-based contrast-enhanced CT (diceCT; Gignac et al., 2016), as I_2KI diffusion renders soft tissues radiodense and produces CNS tissue contrast similar to magnetic resonance imaging (Gignac and Kley, 2018).

2.2. Scanning

Following staining, the brainstem, diencephalon, and cerebellum were dissected from the cerebral hemispheres and microCT scanned at the MicroCT Imaging Consortium for Research and Outreach facility at the University of Arkansas. Scans were obtained using a Nikon X TH 225 ST microCT scanning system outfitted with a 225 kV rotating target, designed to enable X-ray penetration of exceptionally dense materials, and a high-resolution 2000 × 2000 pixel detector. The target was fitted with a 1.5 mm copper filter to decrease the entrance surface dose of the high-powered X-rays, effectively reducing back-scatter and other surface artifacts. Two scanning protocols were used due to limitation of beam-time: a highest resolution protocol (N = 1) and a high-resolution protocol (N = 3). For the highest resolution protocol, the brainstem and cerebellum were scanned at 57.9 μm—a scale comparable to the previous highest resolution MRI scan of a cadaveric brainstem (Calabrese et al., 2015; Edlow et al., 2019; Rushmore et al., 2020)—with X-ray power settings of 190 kV and 255 μA. For X-ray image capture, exposure timing was set to 708 ms, with 12 dB gain, reduction of ring artifacts, and an optimization of projections, with 4 frames averaged per projection. For the high-resolution protocol, the brainstem and cerebellum were scanned at 74 μm, with X-ray power settings of 190 kV and 389 μA. Image capture settings included an exposure timing of 2000 ms, with 12 dB gain, reduction of ring artifacts, and an optimization of projections, with 4 frames averaged per projection. The settings of both protocols ensured maximum contrast of the central nervous system tissues while minimizing X-ray artifacts relative to voxel size (following Gignac et al.,

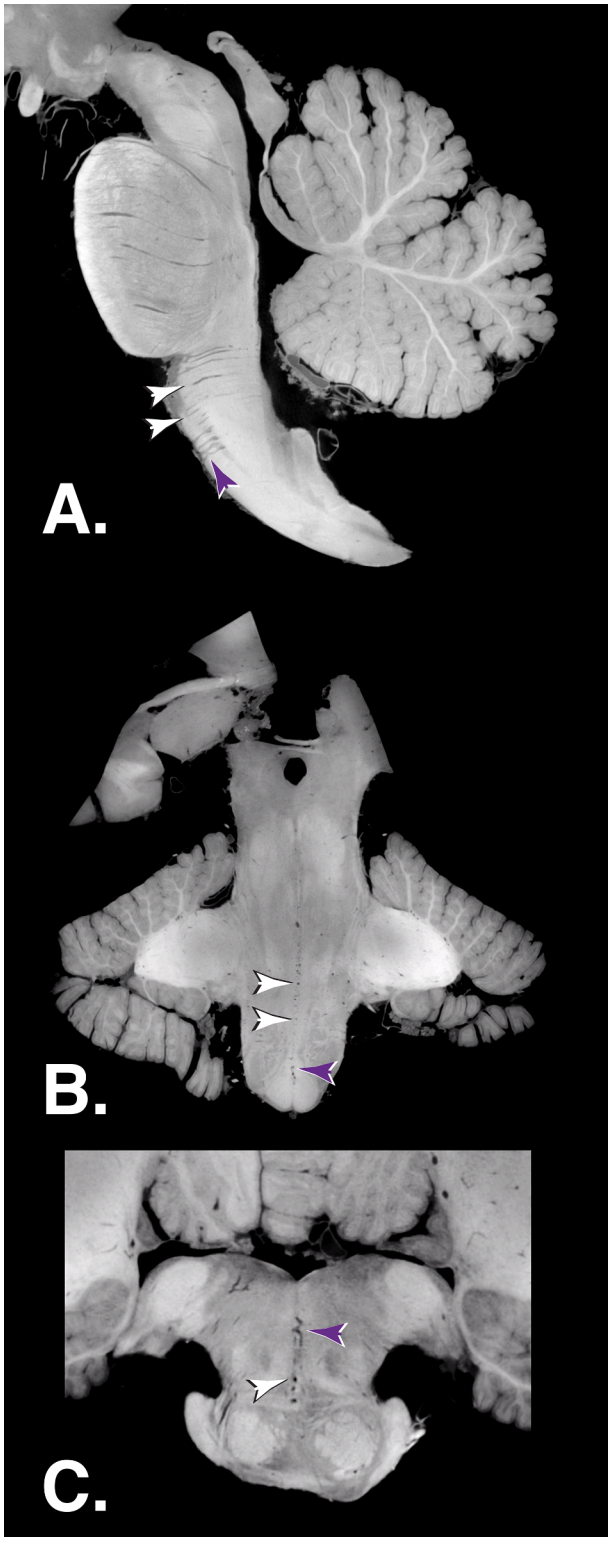

Fig. 1. Cross-Sectional Anatomy. Exemplar cross-sections of the highest-resolution diceCT contrast-enhanced cadaveric brainstem in (A) sagittal, (B) coronal, and (C) horizontal orientations. Contrast between white and gray matter is clear, and penetrating branches of the anterior spinal artery (confirmed by direct branching or circular cross-section) are visible (white arrows). Purple arrows indicate regions of anastomosis in cross-section. (For interpretation of the references to colour in this figure legend, the reader is referred to the web version of this article.)

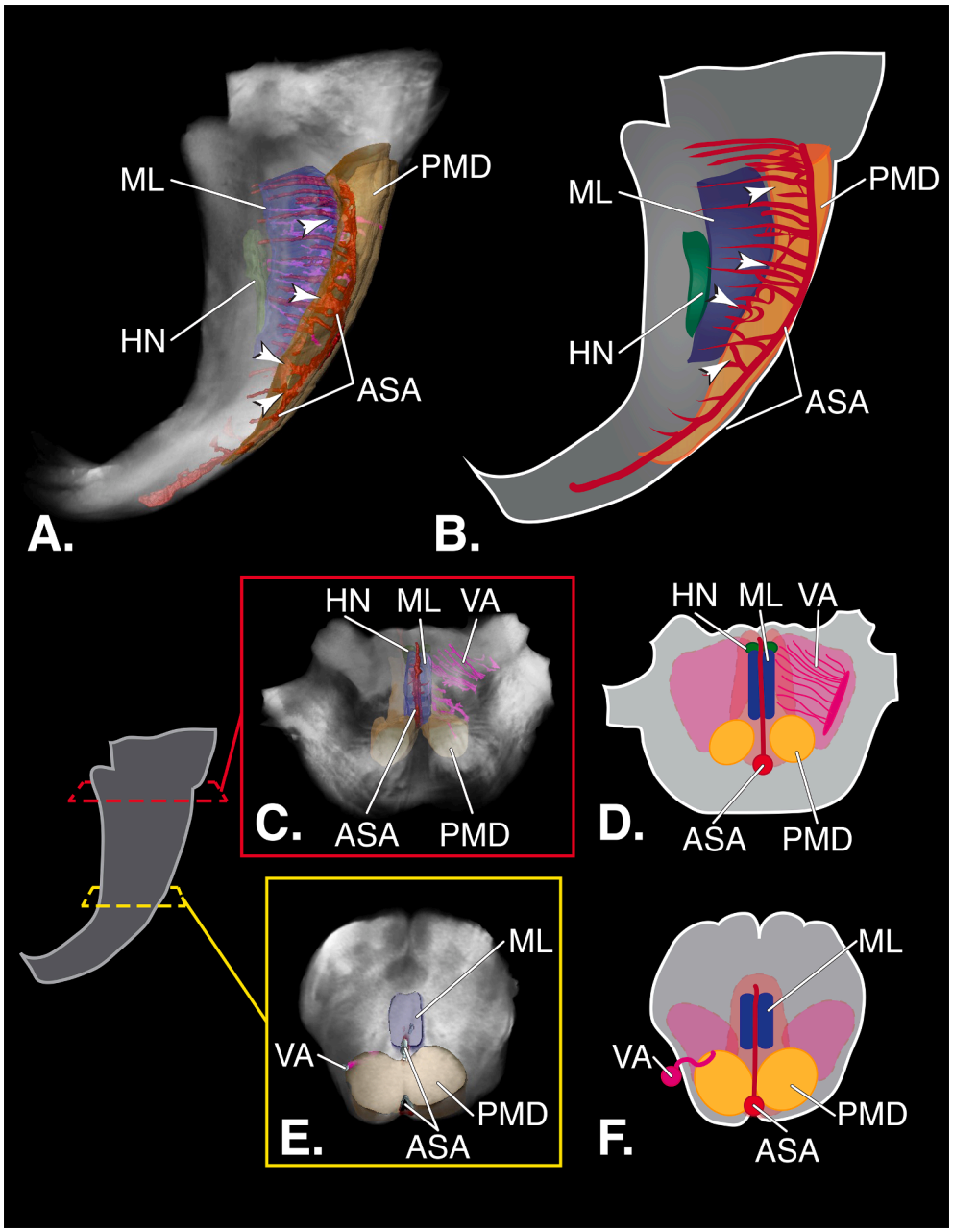

Fig. 2. Digital Dissection and Schematics of the Medulla. Digital segmentation of the neurovascular anatomy of medial medullary syndrome. From the lateral perspective, digital dissection (A) reveals numerous anastomoses of the anterior spinal artery primarily deep to the pyramidal tract (white arrows), re-traced in schematic (B) for clarity. These parallel, branches supply the descending motor corticospinal tracts (pyramids; gold), ascending sensory medial lemniscus (blue), and hypoglossal motor nucleus (green). Similar anastomoses are not observed in reconstruction of the penetrating branches of the vertebral artery (upper or open medulla: C, segmentation; D, schematic). The vertebral artery does not ramify the medial lemniscus in the caudal or closed medulla (E, segmentation; F, schematic). *Abbreviations*: ASA, Anterior Spinal Artery; HN, Hypoglossal Nucleus; ML, Medial Lemniscus; PMD, Pyramidal Tract; VA, Vertebral Artery. (For interpretation of the references to colour in this figure legend, the reader is referred to the web version of this article.)

2016; Gignac and Kley, 2018).

2.3. Segmentation

The image stacks were then used to guide 3D segmentation of the penetrating of the anterior spinal and vertebral arteries, along with relevant surrounding structures in the caudal medulla, using Avizo 2020.1 (ThermoFisher Scientific, Waltham, MA). Because we used diceCT methods and not vascular injection, the arterial trees were segmented by in-filling the negative space of arterial perforations by parent artery territory. Arteries were confirmed by following the anterior spinal artery (present in all specimens) into the tissue, as well as in-filling circular spaces. Spaces with oblong, ovoid, and/or irregular lumina were interpreted to be veins and excluded. The white matter tracts of the lateral corticospinal tract and medial lemniscus, as well as the gray matter hypoglossal nuclei, were digitally dissected by tracing areas of high and low brightness. Segmentation was performed using a combination of automated and manual tools, including histogram-based thresholding and manual segmentation using a digital lasso or paintbrush. The resultant 3D models were then visually analyzed. Segmentation was performed initially by first author (KF) and replicated by senior author (HO). All models were found to be congruent between researchers. Final images were rendered by KF and reviewed against image stacks by KF, PG, and HO.

3. Results

The diceCT methods produced X-ray microCT images of the *ex-vivo* brainstems with distinctive contrast and fine resolution, from which white and gray matter are easily distinguished (Fig. 1). Perforations indicating arterial supply are clear (Fig. 1). Utilizing the methodology described above, a three-dimensionally rendered model of the anterior spinal and vertebral arteries and their tributaries supplying the medial medulla were generated for each brainstem (Fig. 2). Anastomoses were

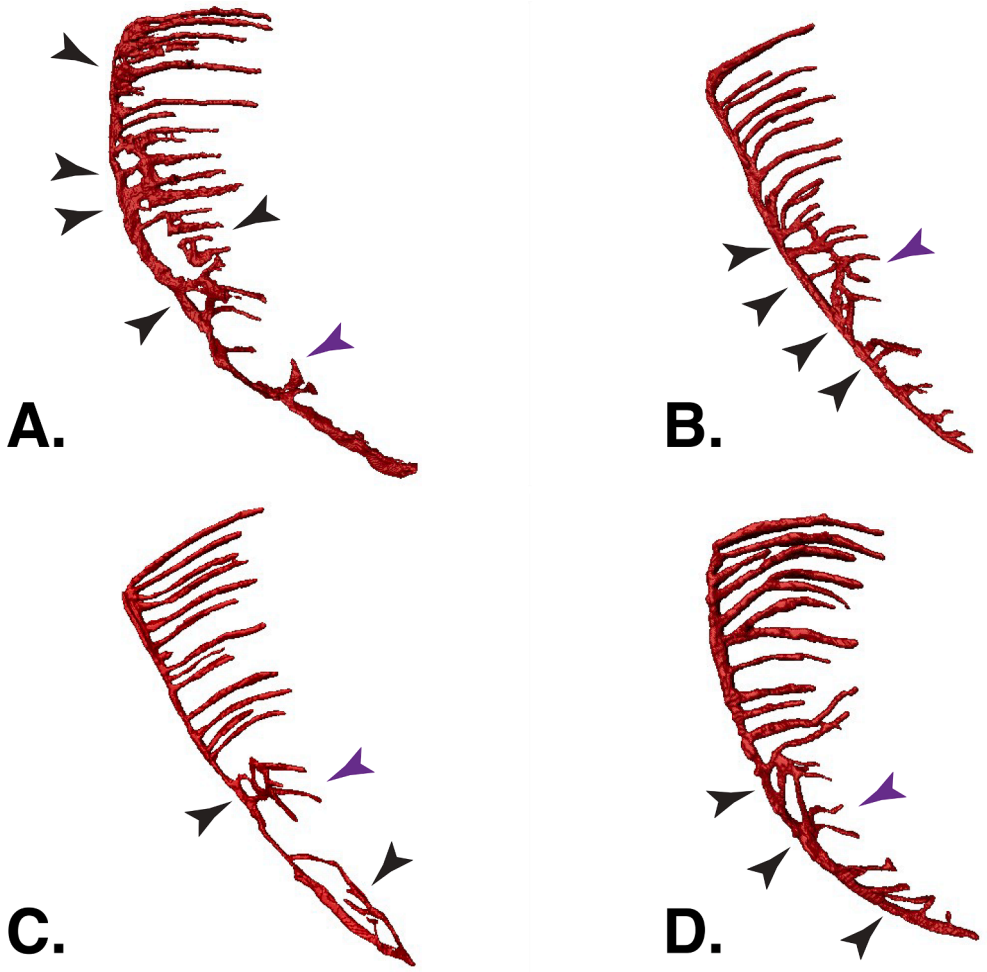

Fig. 3. Variation in Anterior Spinal Artery Territories. Anterior spinal artery segmentation of all four brainstem specimens (A, highest resolution; B–D, high resolution) reveals sites of anastomosis in each (black arrows), as well as laterally-flaring branches that cross the midline at the level of the decussation of the pyramids (purple arrows). (For interpretation of the references to colour in this figure legend, the reader is referred to the web version of this article.)

not identified in the vertebral artery penetrating branches (Fig. 2). Within the anterior spinal artery territory implicated in MMS, numerous small sulcal arteries were visualized perforating the medulla within the anterior median fissure (Figs. 1, 2). As expected, these branches proceed in a parallel and segmental fashion through the anteroposterior depth of the medulla supplying the medullary pyramids, medial lemniscus, and hypoglossal nucleus (Figs. 1–3). Segmental branches are high in density, and penetrate the entire depth of the basal-plate-derived regions of the spinal cord and medulla anterior (ventral) to the central canal and fourth ventricle. Because of the under-representation of alar-plate-derived tissue in the medial medulla due to the opening of the fourth ventricle, these midline branches supply the majority of the midline tissues in the middle and upper medulla. The midline branches were found to be restricted to basal-plate-structures in their distribution, but nonetheless supply the majority of the medulla due to the low representation of alar plate structures in the midline due to the opening of 4th ventricle. In each brainstem, many of the midline arterial branches were found to supply the hypoglossal nuclei; however, these nuclei were also found to receive collateral supply from penetrating branches of the vertebral arteries. Surprisingly, an extensive network of intraparenchymal, rostrocaudal anastomoses between many of the sulcal perforating branches was also visualized in all four samples (Figs. 2, 3). More specifically, this anastomotic network was found parallel to the deep boundary of the pyramids and was present to some degree in all four scanned brainstems (Fig. 3). At the decussation of the pyramids, arterial branches from the midline anterior spinal artery cross and proceed laterally alongside the medial margins of the pyramidal tracts (Fig. 3).

4. Discussion

To our knowledge, this intraparenchymal anastomosis of perforating sulcal arteries within the caudal medulla anterior spinal artery territory has never been described. At their most distal extent, the anterior spinal artery and sulcal arteries are known to form the cruciate anastomosis of the conus medullaris of the spinal cord. However, this arterial basket represents the joining of the anterior and posterior spinal arteries and is rarely described as having an intraparenchymal component (Rojas et al., 2018). Further, the medullary anastomosis described here represents a plausible anatomic basis for the infrequency of MMS, especially in regard to the anterior spinal artery territory. The collateral supply of oxygenated blood flow through this anastomotic network could conceivably render this region of the medulla more resistant to ischemia and subsequent infarction. Although these results are derived from infilling negative arterial spaces within the neural parenchyma, it is unlikely that the connections between segmental arteries represent arteriovenous anastomoses or connections between the arterial and venous systems. Because of the scan resolution (59.7 μm), this study excludes visualization of arterioles and venules (<50 μm), which are difficult to distinguish without histological imaging. Thus, the vessels

can be discriminated based on gross morphology. Moreover, blood vessel connections are between parallel penetrating branches of the same parent artery, and do not resemble arteriovenous shunts (originally described by Rowbotham and Little, 1965). The 3D architecture of this network superficially resembles precapillary arteriovenous anastomoses; however, vessels participating in these anastomoses are within 6–25 μm in external diameter (Hasagewa et al., 1967).

The embryological factors driving the development of this network remain unclear. A possible explanation lies in the stimulatory effect of non-pathologic hypoxia on angiogenesis. The role of hypoxia and hypoxia-inducible factors (HIFs) in upregulation of pro-angiogenic factors, such as vascular endothelial growth factor (VEGF), has been well studied (Fong, 2008; Nanka et al., 2006; Krock et al., 2011). A diffuse expression of VEGF in the developing neural tube (Fong, 2008; Nanka et al., 2006) may help to explain the extensive vascular network we have observed. Additionally, the migration of the brainstem nuclei during development may also help to explain our observations. More specifically, this anastomosis may serve to supply the developing motor nuclei of the basal plate as they migrate medially in the anteroposterior direction.

Our study is limited by the number of cadaver brainstems currently scanned at high enough resolution to elucidate the microvascular networks of the caudal medulla. Further cadaveric scans and 3D reconstructions are needed to better document the frequency and extent of the intraparenchymal anastomoses we have observed. In proposing an anatomical basis for the infrequency of MMS, we hope to underline the increasing quality of imaging techniques and promote their unique ability to interrogate anatomic contributions to vascular phenomena.

5. Contributions

HO conceptualized the study and organized all training. PG and HO prepared and scanned the specimens. KF and HO participated in segmentation. KF, YO, PG, and HO contributed to data analysis and write the final paper. KF and HO submitted the paper for publication. All four authors approve of the paper in its final form.

6. Key points

Question: Is there an anatomical basis for the relative infrequency of medial medullary syndrome (MMS)?

Findings: Within the territory of small sulcal anterior spinal artery branches perforating the medulla within the anterior median fissure, there is a significant network of intraparenchymal, rostrocaudal anastomoses between these perforating branches.

Meaning: This intraparenchymal network may provide a significant collateral supply of oxygenated blood flow throughout the medial medulla, hence contributing to the infrequency of MMS.

Funding

This work was supported by the National Science Foundation [NSF BCS-1725925]; Oklahoma State University Center for Health Sciences; and Oklahoma State University College of Osteopathic Medicine.

CRediT authorship contribution statement

Kaylea M. Feldman: Conceptualization, Methodology, Validation, Investigation, Visualization, Writing – original draft, Writing – review & editing. **Yasmin A. O'Keefe:** Conceptualization, Validation, Writing – review & editing. **Paul M. Gignac:** Conceptualization, Methodology, Validation, Investigation, Data curation, Writing – original draft, Writing – review & editing, Funding acquisition. **Haley D. O'Brien:** Conceptualization, Methodology, Validation, Investigation, Writing – original draft, Writing – review & editing, Visualization, Supervision, Project administration, Funding acquisition.

Declaration of Competing Interest

The authors declare that they have no known competing financial interests or personal relationships that could have appeared to influence the work reported in this paper.

Data availability

The authors do not have permission to share data.

Acknowledgements

We thank the OSU Center for Health Sciences Body Donors who contributed the important anatomical gifts that made this research possible, as well as willed body program manager Thom Garrison and director Dr. Kent Smith. We thank Drs. Kenneth Miller (deceased), Kent Smith, and Nedra Wilson for their advisory role with regard to Oklahoma State Anatomical Board policies and procedures. Scanning at UArk MICRO was assisted by Manon Wilson, and digital rendering was assisted by Dr. Alexander Claxton. Funding was provided to HDO, PMG, and KF by OSU-CHS and the National Science Foundation (NSF BCS-1725925) to HDO and PMG.

References

Bassetti, C., Bogousslavsky, J., Mattle, H., Bernasconi, A., 1997. Medial medullary stroke: report of seven patients and review of the literature. Neurology 48 (4), 882–890. https://doi.org/10.1212/wnl.48.4.882. PMID: 9109872.

Currier, R.D., Giles, C.L., Dejong, R.N., 1961. Some comments on Wallenberg's lateral medullary syndrome. Neurology 11, 778–791. https://doi.org/10.1212/wnl.11.9.778. PMID: 13718920.

Edlow, B.L., Mareyam, A., Horn, A., Polimeni, J.R., Witzel, T., Tisdall, M.D., Augustinack, J.C., Stockmann, J.P., Diamond, B.R., Stevens, A., Tirrell, L.S., Folkerth, R.D., Wald, L.L., Fischl, B., van der Kouwe, A., 2019. 7 Tesla MRI of the ex vivo human brain at 100 micron resolution. Sci. Data 6 (1), 244. https://doi.org/10.1038/s41597-019-0254-8. PMID: 31666530; PMCID: PMC6821740.

Fong, G.H., 2008. Mechanisms of adaptive angiogenesis to tissue hypoxia. Angiogenesis 11 (2), 121–140. https://doi.org/10.1007/s10456-008-9107-3. Epub 2008 Mar 10 PMID: 18327686.

Fukuoka, T., Takeda, H., Dembo, T., Nagoya, H., Kato, Y., Deguchi, I., Maruyama, H., Horiuchi, Y., Uchino, A., Yamazaki, S., Tanahashi, N., 2012. Clinical review of 37 patients with medullary infarction. J. Stroke Cerebrovasc. Dis. 21 (7), 594–599. https://doi.org/10.1016/j.jstrokecerebrovasdis.2011.01.008. Epub 2011 Mar 4 PMID: 21376629.

Gignac, P.M., Kley, N.J., Clarke, J.A., Colbert, M.W., Morhardt, A.C., Cerio, D., Cost, I.N., Cox, P.G., Daza, J.D., Early, C.M., Echols, M.S., Henkelman, R.M., Herdina, A.N., Holliday, C.M., Li, Z., Mahlow, K., Merchant, S., Müller, J., Orsbon, C.P., Paluh, D.J., Thies, M.L., Tsai, H.P., Witmer, L.M., 2016. Diffusible iodine-based contrast-enhanced computed tomography (diceCT): an emerging tool for rapid, high-resolution, 3-D imaging of metazoan soft tissues. J. Anat. 228 (6), 889–909. https://doi.org/10.1111/joa.12449.

Gignac, P., Kley, N., 2018. The utility of DiceCT imaging for high-throughput comparative neuroanatomical studies. Brain Behav. Evol. 91 (3), 180–190.

Hasegawa, T., 1967. Precapillary arteriovenous anastomoses: "thoroughfare channels" in the brain. Arch. Neurol. 16 (2), 217.

Kataoka, S., Hori, A., Shirakawa, T., Hirose, G., 1997. Paramedian pontine infarction. Neurological/topographical correlation. Stroke 28 (4), 809–815. https://doi.org/10.1161/01.str.28.4.809. PMID: 9099201.

Kim, J.S., 2003. Pure lateral medullary infarction: clinical-radiological correlation of 130 acute, consecutive patients. Brain 126 (Pt 8), 1864–1872. https://doi.org/10.1093/brain/awg169. Epub 2003 May 21 PMID: 12805095.

Kim, J.S., Lee, J.H., Suh, D.C., Lee, M.C., Spectrum of lateral medullary syndrome. Correlation between clinical findings and magnetic resonance imaging in 33 subjects. Stroke. 1994 Jul;25(7):1405–10. doi: 10.1161.01.str.25.7.1405. PMID: 8023356.

Kim, J.S., Kim, H.G., Chung, C.S., 1995. Medial medullary syndrome. Report of 18 new patients and a review of the literature. Stroke 26 (9), 1548–1552. https://doi.org/10.1161/01.str.26.9.1548. PMID: 7660396.

Krock, B.L., Skuli, N., Simon, M.C., 2011. Hypoxia-induced angiogenesis: good and evil. Genes Cancer 2 (12), 1117–1133. https://doi.org/10.1177/1947601911423654. PMID: 22866203; PMCID: PMC3411127.

Merwick, Á., Werring, D., Posterior circulation ischaemic stroke. BMJ. 2014;348:g3175.

Nanka, O., Valásek, P., Dvoráková, M., Grim, M., 2006. Experimental hypoxia and embryonic angiogenesis. Dev. Dyn. 235 (3), 723–733. https://doi.org/10.1002/dvdy.20689. PMID: 16444736.

Ng, Y.S., Stein, J., Ning, M., Black-Schaffer, R.M., 2007. Comparison of clinical characteristics and functional outcomes of ischemic stroke in different vascular

territories. Stroke 38 (8), 2309–2314. https://doi.org/10.1161/STROKEAHA.106.475483. Epub 2007 Jul 5 PMID: 17615368.

Paciaroni, M., Silvestrelli, G., Caso, V., Corea, F., Venti, M., Milia, P., Tambasco, N., Parnetti, L., Gallai, V., 2003. Neurovascular territory involved in different etiological subtypes of ischemic stroke in the Perugia Stroke Registry. Eur. J. Neurol. 10 (4), 361–365. https://doi.org/10.1046/j.1468-1331.2003.00646.x. PMID: 12823486.

Rojas, S., Ortega, M., Rodríguez-Baeza, A., 2018. Vascular configurations of anastomotic basket of conus medullaris in human spinal cord. Clin. Anat. 31 (3), 441–448. https://doi.org/10.1002/ca.22986. Epub 2017 Oct 27 PMID: 28906042.

Rowbotham, G.F., Little, E., 1965. A new concept of the circulation and the circulations of the brain. The discovery of surface arteriovenous shunts. Brit J Surg. 52 (7), 539–542.

Toyoda, K., Imamura, T., Saku, Y., Oita, J., Ibayashi, S., Minematsu, K., Yamaguchi, T., Fujishima, M., 1996. Medial medullary infarction: analyses of eleven patients. Neurology 47 (5), 1141–1147. https://doi.org/10.1212/wnl.47.5.1141. PMID: 8909419.

Vuilleumier, P., Bogousslavsky, J., Regli, F., 1995. Infarction of the lower brainstem. Clinical, aetiological and MRI-topographical correlations. Brain 118 (Pt 4), 1013–1025. https://doi.org/10.1093/brain/118.4.1013. PMID: 7655878.